

11.07.2016

Alen Mujkanović
alenmu@student.ethz.ch
+41 78 730 75 32**Semester Project FS16**

Real-time Gradient Impulse Response Function Harvesting

Abstract

The following work demonstrates the feasibility of a highly accurate method for continuous characterization of MR gradient system responses, with a focus being laid on modelling the nature of thermal drifts observed in such systems. Continuous characterization is typically subject to strenuous hardware requirements and complex measurement setups. The presented method is based on sparse intermittent field probe measurements, which allows significantly reducing the field monitoring HW requirements while retaining accuracy. This is achieved through underlying assumptions on the physical properties of the system: a limited number of significant eddy current and mechanical oscillation terms causing response deviations as well as slow time-variance induced by gradient coil heating (over a few minutes). For suitable sequences, a maximum characterization error of 0.07% – 0.2% of the peak input gradient strength compared to continuous field monitoring is achieved. The characterized system imperfections are important impediments in the image quality of non-Cartesian and rapid imaging sequences, as well as specialized applications such as diffusion imaging. Furthermore, an accurate continuous characterization could allow real-time pre-emphasis optimization or offer a means for quality assurance.

Supervisors: Bertram Wilm, Institute for Biomedical Engineering, ETH Zürich
Klaas Prüssmann, Institute for Biomedical Engineering, ETH Zürich

Introduction

Spatiotemporal variation of magnetic field gradients is a principal mechanism in MR signal encoding, hence, knowledge of the entirety of the field progression and with it the k -space trajectory is of crucial importance in interpreting acquired signals and consequent image reconstruction (1). The diagnostic quality of many MR imaging techniques heavily relies on the accuracy of the k -space trajectories. For sensitive applications even small deviations from the expected trajectories can cause severe detrimental effects on image quality. Various artifacts have been observed in a number of common imaging procedures and methods. Moreover, these accuracy limitations become increasingly pronounced at higher field strengths and hence provide additional motivation to find solutions for use in ultra-high field MRI. Several compensation methods have been developed and are in routine use for quite some time, but remaining significant imperfections continue to be an issue. Limited gradient accuracy still poses a barrier in the adoption of techniques theoretically offering shorter scan times through higher encoding efficiency. Sequence modification for particular applications can remediate some of the issues by decreasing sensitivity to field inaccuracies, but such solutions are not always applicable and provide other drawbacks such as the need for longer or repeated readouts. Due to the similar nature and dynamic behavior of gradient and shimming systems currently in use, parts of the presented work directly apply or can be expanded to shim systems and shim characterization can be performed similarly, as has been demonstrated previously (2).

Due to the structure of the gradient hardware and complex interplay with other system components, several perturbations of differing physical origin of gradient dynamics occur, caused in large part by hardware imperfections. There are various principle limitations and deficiencies of the hardware, such as amplifier bandwidth and linearity limitations, gradient delays (3), eddy current induction in gradient coils and the surrounding conducting

structures (4–7), mechanical vibrations producing field fluctuations (8), mutual coupling of gradient channels (9,10) and drifts of these effects caused by heating of the gradient coils (3). Further irreproducible dynamic field fluctuations caused by patient motion during in vivo experiments (11,12) or external magnetic sources and currents could possibly occur as well (13). Uncompensated field deviations give rise to notable ghosting artifacts and distortion in EPI sequences (14,15) and blurring in spiral imaging (16), among others. Advanced readout trajectories, as used in single-shot, interleaved or non-Cartesian acquisition, requiring high gradient field strengths and fast switching, particularly suffer from large eddy current effects. Temperature effects have been shown to have a significant impact on quantitative phase-contrast and flow imaging (17), whereas mechanical oscillations are known to cause modulation sidebands in MR spectroscopy (18). The principles used in highly-specialized imaging techniques often impose more stringent requirements on fidelity of individual readouts, overall scan time and SNR. Examples of such methods and their sensitivity to dynamic field perturbations have been identified among others in phase-contrast techniques common in cardiovascular imaging applications (17), spectroscopic MRI, functional MRI (19) and diffusion imaging (20).

These dynamic perturbations can and have been addressed in several ways with varying results. Sequence design strategies which allow reducing the sensitivity to perturbations are used, for example in correcting phase inconsistencies between alternating readout lines in EPI. These are only applicable in suitable cases and come at the expense of longer acquisition, reducing their attractiveness for certain applications. Apart from continuous hardware optimization, which is bound to reach physical limits, approaches attempting exact prediction of k -space trajectories have shown success (21–24). Hereby a natural assumption of linearity and time-invariance is utilized to characterize gradient responses (3,25). A logical conclusion of an LTI system is the existence of a *gradient impulse response function (GIRF)*, which has recently been

introduced and successfully applied to quantify all significant deviations from the ideal response (13). An accurate prediction of gradient behavior can be of great value in sequence design, can be used to optimize preemphasis parameters or after acquisition for image reconstruction. Despite the simplicity and excellent results of such an assumption allowing fast and robust implementation in image reconstruction, not all of the above effects can be described in this fashion. Heating effects, patient movement and external field sources cannot be described within an LTI model of gradient response. Of the response deviations breaking with the LTI assumption, thermal drifts pose the most significant contribution, having been shown to cause gradient timing errors of over a millisecond to the nominal time-course (3), an effect exacerbated in long scans or techniques with high gradient duty cycles, as found in single-shot readout sequences.

Strategies that do not rely on assumptions or prior knowledge of the response have also been used to tackle the issue of lacking gradient fidelity. These are procedures that directly measure or estimate *k*-space trajectories for improved image reconstruction (26,27). Such methods, relying on sequence modification and multiple acquisitions for each gradient, pose certain drawbacks concerning accuracy and prolonged acquisition times. A more recent approach is the direct measurement of the gradient field evolution with specialized hardware, i.e. several NMR field probes termed field monitoring (28). Different monitoring approaches have been developed with increasingly sophisticated hardware (9,29–35). Concurrent field monitoring makes assumptions on time-invariance and linearity unnecessary by providing a method to capture the entire spatiotemporal field evolution in parallel to the actual data acquisition. This allows a separation of sequence design and field characteristics. However, it also increases the complexity of data acquisition. Furthermore, the additional hardware requirements can be substantial. MR field monitoring is based on acquisition of free induction decay (FID) signals from each of the field probes. The accrued phase of the probe FID signal correlates with

the integral of the field progression and can be derived thereof. In a typical concurrent field monitoring setup, several T/R probes are arranged around the imaging volume which is nearly perfectly free of any dynamic field perturbation sources and can hence be expanded into a small set of spherical harmonic functions which fully characterize dynamic field contributions up to a given spatial order (29) dependent on the number of probes used. The field data is used to determine a best-fit of time-varying coefficients for the spherical harmonic basis.

In the case of ¹H imaging the most effective way to avoid disturbances between monitoring and image data acquisition is to rely on heteronuclear spectral decoupling by using a different sample material in the probes, commonly containing ¹⁹F (9,10,15) or ²H (32). This also requires heteronuclear T/R capabilities of the utilized spectrometer or a dedicated system. Due to coherence loss, the signal readout length is limited and is on the order of probe *T*₂, which can reach values of around 100 ms with proper susceptibility matching (30,31,36). This limits field monitoring with long-lived probes to sequences of this time-scale or to operation in a pulsed regime, where long relaxation times necessary between successive probe excitations cause gaps in the monitored signal. Coherent probe excitation schemes can alleviate this issue partially with somewhat increased hardware requirements (33). For reproducible gradient effects this problem can also be addressed through repeated shifted measurements on a sliding window principle at the cost of scan time. Concurrent ¹H monitoring usually requires RF-shielding to reduce interference between the imaging and monitoring experiments (37) which can also shield HF gradient responses (31,32). An approach using extremely short-lived ¹H probes (*T*₁ ≈ 160 μs) and rapid re-excitation of alternating probe sets was demonstrated recently (35). Due to fast relaxation, this setup enables monitoring sequences with large gradient moments which is challenging with long-lived probes. However, the results come with formidable demands on the acquisition system.

The present study is aimed at providing a method for continuous high-fidelity gradient chain characterization with low hardware requirements. This is achieved with a numerical optimization approach (38) by leveraging knowledge of the physical origin and properties of the field deviations and combining it with information gained from intermittent concurrent field monitoring. The concept is based on the hypothesis that the overall response can be accurately predicted with by a composition of a time-invariant and slow time-variant part. A physical model is continuously fitted to data acquired by low measurement duty cycle monitoring, i.e. containing large readout gaps. The overall time-invariant response including remaining imperfections such as amplifier limitations, which cannot be accurately modeled, are captured in a prior calibration step. This response, the $\alpha GIRF$, forms the basis upon which the continuously adjusted $\Delta GIRF$ is superposed to regain the full slowly time-varying gradient response. The validity of the hypothesis is evaluated and the overall characterization method is compared to other established approaches.

Theory

Time-Variant Response Separation

The concept of characterizing the gradient chain response as an LTI system and the consequence of such an assumption being the existence of a GIRF completely describing the linear system response as briefly introduced earlier on, is fully adopted from previous studies (13) and expanded to allow continuous response adaptation caused by slow temperature variation. For such a system, the following relation can be used to determine the response to any given input, given the duration lies below the timescale of significant gradient heating:

$$o(t) = i(t) * g(t) = \int_{-\infty}^{\infty} i(\tau) \cdot g(t - \tau) d\tau, \quad [1]$$

where $i(t)$, $o(t)$ and $g(t)$ denote the prescribed gradient time-course, actual system output and GIRF in the time domain, respectively. Knowing the

impulse response equates to knowing the response $O(\omega)$ to any given input, which is determined by simple multiplication of the input $I(\omega)$ with the impulse response $G(\omega)$ in Fourier space:

$$O(\omega) = I(\omega) \cdot G(\omega). \quad [2]$$

Our model additionally assumes the existence of small time-varying components of the gradient response, thus relaxing the strict time-invariance assumption. The time-invariant components shall be represented by $\alpha G(\omega)$ and the time-varying components by $\Delta G(\omega, \tau)$, named due to its nature of representing the difference between two impulse responses evaluated at different points in time. At any given instance τ , the system can accurately be represented by the superposition of the responses:

$$O(\omega) = I(\omega) \cdot [\alpha G(\omega) + \Delta G(\omega, \tau)]. \quad [3]$$

This separation was selected after initial efforts at achieving continuous characterization of the full GIRF with the underlying physical method and numeric implementation resulted in an unsatisfactory outcome, particularly in the high frequency range of responses. Instead, $\alpha G(\omega)$ must be acquired in a calibration step where a variety of methods, as described above, can be utilized to achieve sufficient results. The calibration step does not need to be performed often, as the response stays eminently stable even over long time-scales of several years (13), disregarding short-scale variations due to temperature fluctuations. Results of both methods investigated, full GIRF prediction and individual $\alpha GIRF$ and $\Delta GIRF$ prediction, are compared and discussed in the following sections, but the focus is laid on obtaining a highly accurate characterization of the time-varying response $\Delta G(\omega, \tau)$.

Physical Model

The utilized approach to continuous gradient characterization heavily relies on prior knowledge of the underlying physical system in order to produce accurate results with limited hardware requirements. Several assumptions based on a physical analysis of the underlying causes for deviations are made. For an ideal gradient system

with zero response delay, infinite bandwidth and absolute fidelity the GIRF would simply be flat and equal to unity with no phase effects in Fourier domain, i.e. represented by a perfect Dirac delta function $\delta(t)$ in time domain. Such an ideal system would replicate the prescribed input at the output. Imperfect gradient behavior causes deviations from this ideal response, which are in turn induced by gradient switching, i.e. changes in the input, motivating the introduction of an additional function $h(t)$ (39) and the following input-output relation:

$$o(t) = i(t) - \frac{d}{dt} i(t) * h(t), \quad [4]$$

which leads to the relation between $h(t)$ and $g(t)$ represented in the Fourier domain as:

$$G(\omega) = 1 - j\omega H(\omega). \quad [5]$$

This newly introduced function could best be described as a gradient *step error response* since it represents the difference between an ideal step response and the actual step response of the gradient system. The importance of this function lies in the fact that it provides a straightforward relation between any deviation terms which are directly induced by gradient switching and the GIRF. Two main kinds of field deviation sources occurring upon gradient switching have been identified in the past: eddy currents in conducting structures and mechanical vibrations of the gradient coils. Upon gradient switching, the rapid change in magnetic field strength in and around the gradient coils will induce electric currents in conducting structures due to Faraday's law. These are manifestations of a certain inertia to changes in the established field equilibrium and hence generate a magnetic field that opposes the applied field, an effect described by Lenz's law. Given the nature of Faraday's law allows concluding that these will be circular currents in planes perpendicular to the applied field that eventually dissipate due to losses. During the initial stage of switching, these effects can be so large that they cause an apparent overall delay in the system response. Due to the significant effect of eddy currents on imaging quality, they have been among the earliest targets for correction,

where primarily preemphasis correction was deployed to reduce the effects of long-lived eddy currents. The physical characteristics of eddy currents have successfully been modeled with a lumped LR-circuit analogy (Figure 1), which gives the characteristic multi-exponential decay observed in the gradient response (4,5). Several eddy currents modeled as exponential decay terms of different time-constants describing remaining eddy currents not compensable through preemphasis correction are included in our physical model:

$$h_{ec}(t) = \sum_n a_n \exp\left(-\frac{t}{\tau_n}\right), \quad [6]$$

where a_n are the amplitudes and τ_n time constants of the n eddy terms. It is important to distinguish between induction effects in differing spatial directions from the driving gradient direction and those in the same direction. Eddy currents that are induced by switching a gradient in a certain spatial direction can have an effect on the field in the same direction, through self-inductance, or on other directions, so-called cross-induction. Several higher order terms of a more complicated spatial dependence can be described in the same spherical harmonic basis as applicable in higher-order field monitoring (9,13). The utilized approach could directly be expanded to characterize cross-induction and higher-order terms, but in the scope of the present work only self-terms have been analyzed.

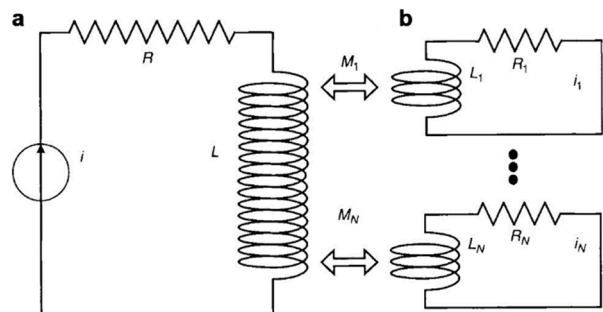


Figure 1. LR-Circuit analogy for eddy currents. The driven gradient coil (a) causes exponentially decaying eddy currents in the surrounding conductors (b) through mutual inductance. Each conductor, as well as the gradient coil is modeled by an LR-circuit, with differing electric properties and by extension decay constants. More complicated cross-coupling effects are hereby typically neglected. Image source Elsevier (39)

Apart from eddy currents, gradient switching also causes a mechanical effect through electromechanical coupling. This causes mechanical vibrations in the audible range (40). Apart from the obvious downside of very high sound levels up to 130 dB, these also cause disturbances of the gradient dynamics (8). Modelling approaches for the oscillations have been used to simulate modulation sidebands in MRS where a simple damped harmonic oscillator or RLC model has been used (22). This essentially leads to a response composed of an underlying sinusoidal oscillation overlaid with an exponentially decaying amplitude similar to the eddy current model (Figure 2). These are visible in plots of frequency dependence of GIRFs as characteristic peaks at the frequency of oscillation and can also be determined by acoustic measurements in the bore. The various vibration terms have a combined response of:

$$h_{mv}(t) = \sum_m b_m \exp\left(-\frac{t}{\theta_m}\right) \cos(\omega_m t + \phi_m) \quad [7]$$

where b_m , θ_m , ω_m and ϕ_m denote the oscillation amplitude, decay constant, frequency and initial phase, respectively.

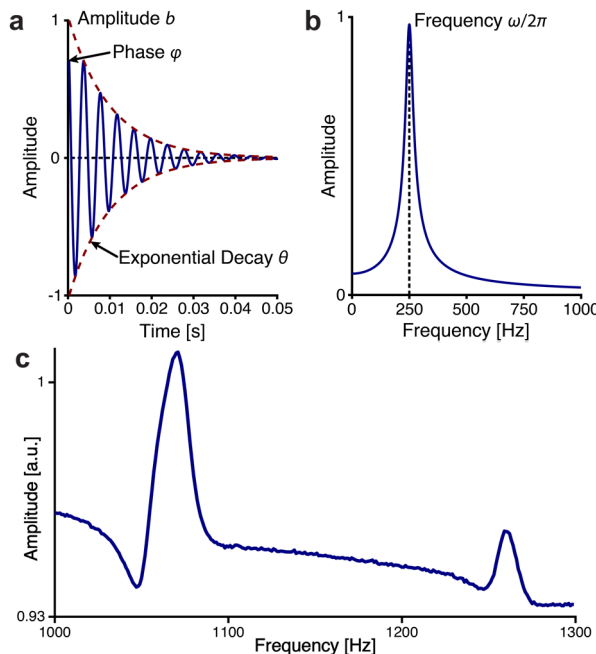


Figure 2: Time (a) and frequency (b) response of a simple harmonic resonator used to model the effect of mechanical vibrations of gradient coils on magnetic field dynamics. Mechanical resonance peaks visible in a GIRF (c)

To complete the step error response model $h(t)$ and by extension $\Delta g(t)$, we need to account for system causality and global gradient delay, hence it is necessary to overlay the response with an ideal step, the Heaviside step function $\sigma(t)$, and shift it by time τ_{delay} . This gives our overall model:

$$h(t) = \delta(t - \tau_{delay}) * [\sigma(t) \cdot (h_{ec}(t) + h_{mv}(t))] \quad [8]$$

Fragmented Output Fitting

The problem has been reduced to finding an accurate representation of $\Delta G(\omega, \tau)$, which could easily be accomplished given the full time course of the input and output gradient waveforms. This is typically the case for the input waveform, but obtaining a sufficiently accurate output estimation for the full duration of a scan, without sequence modification or loss in accuracy, is a challenging task, necessitating an elaborate setup, such as demonstrated in (35). It is however, possible to concurrently monitor the output with lower HW requirements if only short fragments of length T_{set} are recorded instead of the full waveform (41). These are interleaved with periods of no signal of length T_{gap} . In contrast, the input waveform is prescribed and thus known in its entirety.

Given the long timescale of relevant gradient heating of a few minutes (17) compared to the length of pulse sequences typically found in MRI, it is not necessary to determine $\Delta G(\omega, \tau)$ for every point in time, rather, it can dynamically be updated, even during an ongoing scan, thereby giving a series of gradually evolving separate impulse responses $\Delta G_i(\omega) = \Delta G(\omega, iT_p)$, where T_p is the update period and $i \in \{1, 2, 3, \dots\}$. Each of these responses are determined in a numerical optimization procedure implementing a solution of the following minimization problem:

$$o'(t) = \begin{cases} 0 & \text{if } t \in \mathbb{T}_{on} \\ \mathcal{F}^{-1}[I \cdot (\alpha G + \Delta G_n)] & \text{else} \end{cases} \quad [9]$$

$$\min_{\vec{p}} \|o(t) - o'(t)\|_2. \quad [10]$$

The $\vec{p} = \{\tau_{delay}, a_{1\dots n}, \tau_{1\dots n}, b_{1\dots m}, \theta_{1\dots m}, \omega_{1\dots m}, \phi_{1\dots m}\}$ vector represents the parameter space for each of

the terms of our physical model: a global delay, n eddy current terms and m mechanical oscillation terms. The procedure is implemented to adapt to the sparse fragmentary nature of the available measured output waveform where the actual waveform was only measured for times $t \in \mathbb{T}_{on}$. Hence, the actual fitting of measured output values $o(t)$ and inferred values $\hat{o}(t)$ is carried out in the time domain, due to the lack of a highly resolved Fourier domain representation, whereas the convolution with the input to obtain $\tilde{o}(t)$ is accomplished by efficient fast Fourier transforms (FFT).

Methods

Experimental Setup

The main aim of the presented study was the reduction of concurrent monitoring hardware demands while retaining the benefits of obtaining full gradient waveforms to a high degree of accuracy in high temporal and spectral resolution, i.e. the exact k -space trajectories. In order to evaluate the viability of the suggested procedure against continuously monitored results the data was acquired with a setup as described in (35). Only parts of the full reconstructed waveforms were actually used to verify the approach, thus mimicking a fragmentary acquisition as would be typically acquired by a less demanding setup. The full dataset was used for comparison and evaluation of the obtained results.

The experiments were carried out in a Philips Achieva 7T whole-body MR system (Philips Healthcare, Best, Netherlands). Data for methods validation and comparison was acquired by a monitoring setup with a field probe array consisting of two sets of 8 ^1H probes each arranged radially on two parallel polytetrafluoroethylene (PTFE) plates forming a cylindrical structure of variable diameter and length (Figure 3a). For optimal monitoring of the first spatial order (B_0, G_x, G_y, G_z), the probes of each set were selected to form two square cuboids rotated by 90° around the central axis of the cylinder (Figure 4). The probe H_2O samples were contained in glass capillaries and doped with $\text{GdCl}_3 \cdot 6\text{H}_2\text{O}$ so that $T_1 \approx 110\mu\text{s}$ and $T_2 \approx 70\mu\text{s}$. Capillary

size was chosen for maximum SNR under consideration of critical dephasing time at the strongest gradient strength. The probe-heads (Figure 3b) and mechanical placement structures were devoid of ^1H sources to avoid signal interferences with the sample. Six windings of PTFE-coated thin copper wire surrounded the capillaries and acted as T/R coils. The capillaries were placed in PTFE holders and an appropriate tuning and matching circuit contained on a PTFE-based printed circuit board (Duroïd, C.I.F, Buc, France) was attached to the coil (Figure 3c). The RF connection for excitation and transmission consisted of 50Ω PTFE dielectric coaxial cables (Multiflex 86, Huber-Suhner, Herisau, Switzerland). A dedicated RF chain and spectrometer adapted from (41) were used for signal acquisition and low-level processing, with further processing on an FPGA based DPS and ensuing methods implementation on a host computer. A schematic overview is displayed in Figure 4, for detailed information on the setup refer to (35).

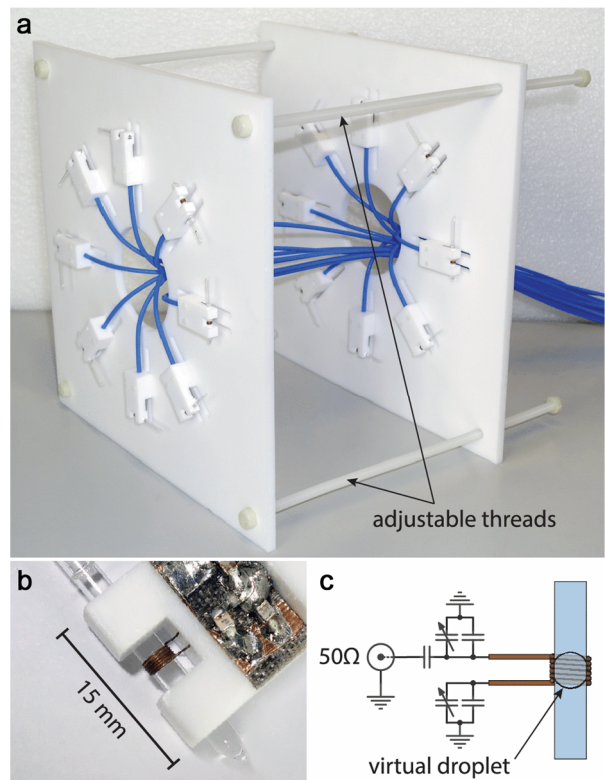


Figure 3: Mounted probe array with 16 ^1H probes and adjustable mechanical frame as utilized in the experiments (a), probe-head circuitry with T/R coil wrapped around capillary (b) and probe design schematic (c). Courtesy of B. Dietrich. Adapted from (35)

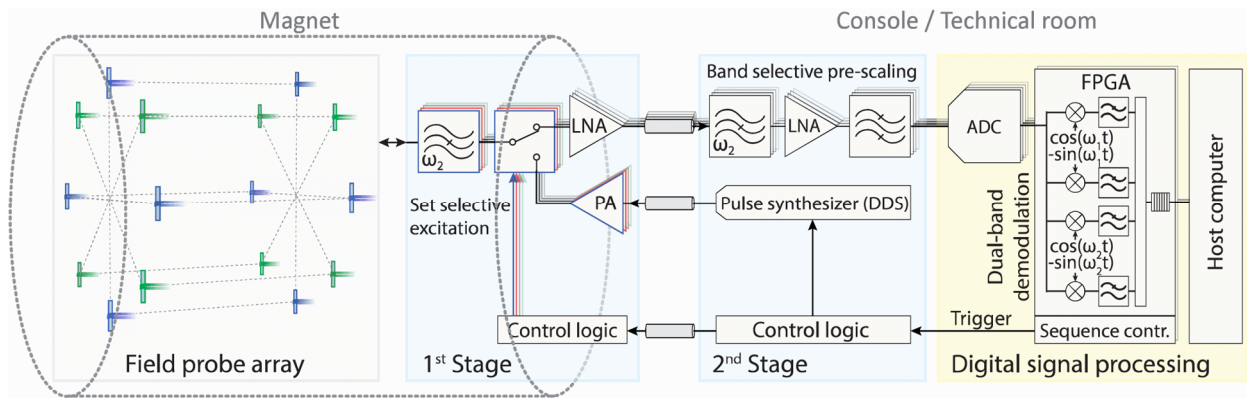


Figure 4: Schematic overview of the field monitoring system utilized. From left to right: field array showing the two probe sets (colored blue and green); 1st stage electronics with filters and T/R switches, afterwards low noise amplifiers (LNA) in the receive path and power amplifiers (PA) for excitation in the transmit path; 2nd stage electronics consisting of anti-aliasing filters and a second amplifier stage in the receive path and direct digital synthesizer (DDS) for RF-pulse generation in the transmit path; digital processing stage with analog-to-digital converters (ADC), FPGA units for demodulation and host computer for control and high-level processing. Courtesy of B. Dietrich. Adapted from (35)

Signal Acquisition and Data Processing

Three types of trajectories were selected for the experiment: adapted frequency sweeps (100 ms, 0 kHz to 30 kHz), unipolar blips, i.e. short triangular impulses (0.31 ms duration) and a 2D-SSh-EPI sequence (132 ms per slice, 1.5 mm resolution). The sweeps and blips were carried out successively for each of the gradient directions (x , y and z). Appropriate input gradient waveforms were generated, where the input was restricted by the MR system to a dwell time of $dt_{in} = 6.4\mu s$. The experiment consisted of repeated successions of these three sequences, alternated with a high gradient duty cycle sequence used to heat the gradient coils and surrounding structures between repetitions, which were not recorded. The experiment was carried out over a timespan of around 45 minutes whereby the temperature was observed to raise up to around 20°C above the starting temperature during the first half, during which additional gradient heating sequences were applied, and return to prior values in the second half, during which the coils were given sufficient time to cool down between the following measurements. In total, 11 sets of the three sequences were acquired capturing gradient characteristics even at temperature ranges which would commonly be reached only during gradient-intense or long scans, such as applied in diffusion MR imaging.

The signals were acquired with a sampling rate of $F_{S,out} = 1MHz$ which equates to a time domain resolution of $dt_{out} = 1\mu s$. The total monitoring duration for each sequence was $T_S = 1.1s$, which includes a long tail after the last gradient switching which was chosen to allow an appropriate frequency domain resolution and it also ensures that any long-lived eddy currents are recorded. From the recorded repeated FIDs of both probe sets, phase data was extracted and used to obtain 1st order gradient terms (G_x , G_y and G_z) through the method described earlier (29). Characterization of static B_0 field inhomogeneity was outside the scope of this work. For later comparison, full waveforms were reconstructed from measurements performed by both probe sets with an alternation period of T_{set} including gaps of length $T_{gap} = 15\mu s$. This was achieved under a 30 kHz BW limitation. For methods evaluation an integer factor q_{gap} was introduced denoting by which amount the data amount was to be reduced. The signal from the first period of length T_{set} was kept and the samples re-coded during the next several periods ($q_{gap} - 1$) · T_{set} were discarded, thereby increasing T_{gap} by the same amount (Figure 5). Thus, monitoring with a single probe-set of short signal life-time and comparatively long relaxation was simulated, such as being possible with weakly doped ¹⁹F probes due to limited solubility of paramagnetic salts.

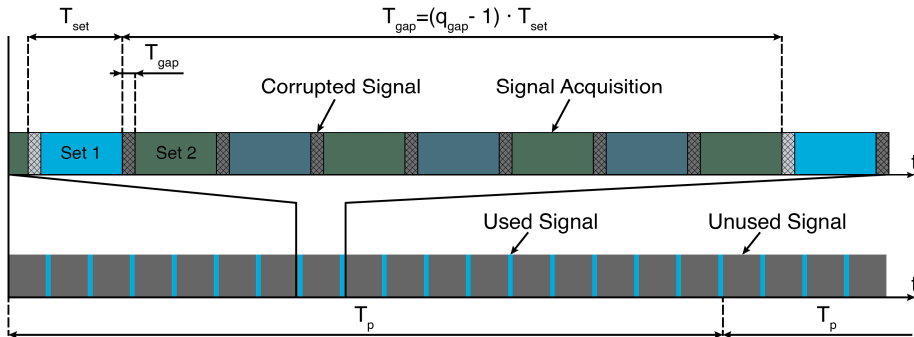


Figure 5: Simple overview of signal timing, illustrating the full acquisition from the different probe-sets with regularly spaced gaps, as well as the effect of increasing the gaps by the factor q_{gap} .

The input and output signals were resampled to a matching resolution in time ($dt_{in} = dt_{out} = 5\mu s$) and in frequency domains ($df_{in} = df_{out} = 1 Hz$), where care had to be taken to avoid truncation of the output signal in the frequency domain due to discontinuities in the time domain. The reduced and resampled signals formed the basis for the minimization problem, as given by equation [10]. The posed problem, based on parameters of the physical model, was formulated in MATLAB and several approaches for solving it were tested. The final implementation uses a constrained gradient descent method implemented by the MATLAB `fmincon` solver, due to speed and robustness considerations. A considerable obstacle for such numerical minimization schemes lies in potentially large parameter spaces \vec{p} . However, according to the hypothesis, the number of significant eddy and vibration terms necessary to model changes in gradient response due to heating is limited. The α GIRF has to be determined from a previously calculated GIRF, which can be gauged by various methods such as phantom measurements, either in a separate calibration step, or as was the case here, directly from the full concurrent monitoring acquisition. In our case, the fully reconstructed gapless output gradient time-course from the first sweep sequence served as the basis to calculate the full GIRF (Figure 6a) by simple division with the input in the Fourier domain (13). Due to the vastly different decay constants (two orders of magnitude) of oscillation and eddy current terms, it is possible to largely remove the vibration contributions by smoothing the GIRF (Figure 6b) through truncation in the time domain. Taking the difference

of the two and applying the optimization algorithm described above allows us to fit several mechanical oscillation terms with very high accuracy (Figure 6c). Finally, the fitted terms are subtracted from the initial GIRF to obtain the α GIRF (Figure 6d). This is essentially a GIRF devoid of mechanical oscillation or thermal effects and serves as a basis for subsequent continuous fitting of the Δ GIRF in intervals of length T_p , capturing the remaining fluctuating effects with just 2 – 4 eddy current terms and a small number of vibration terms (up to 10). A further advantage of the approach is that the determined physical parameters of the vibrations can serve as starting points for fitting these terms after drifting, the implicit assumption being that changes in physical properties of the system are continuous and gradual with steady heating. This is a key principle of continuous characterization via iterative adjustments of model parameters.

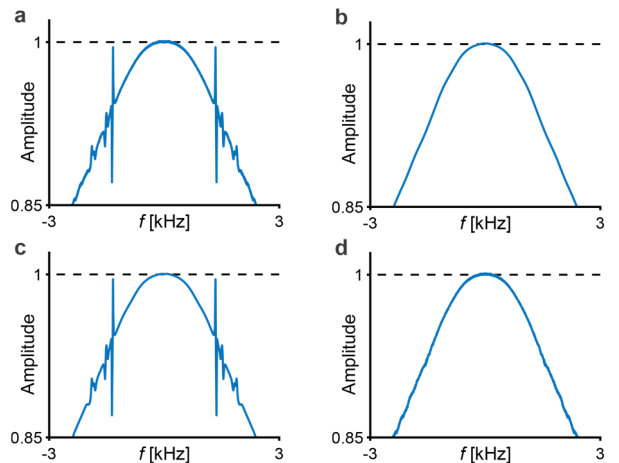
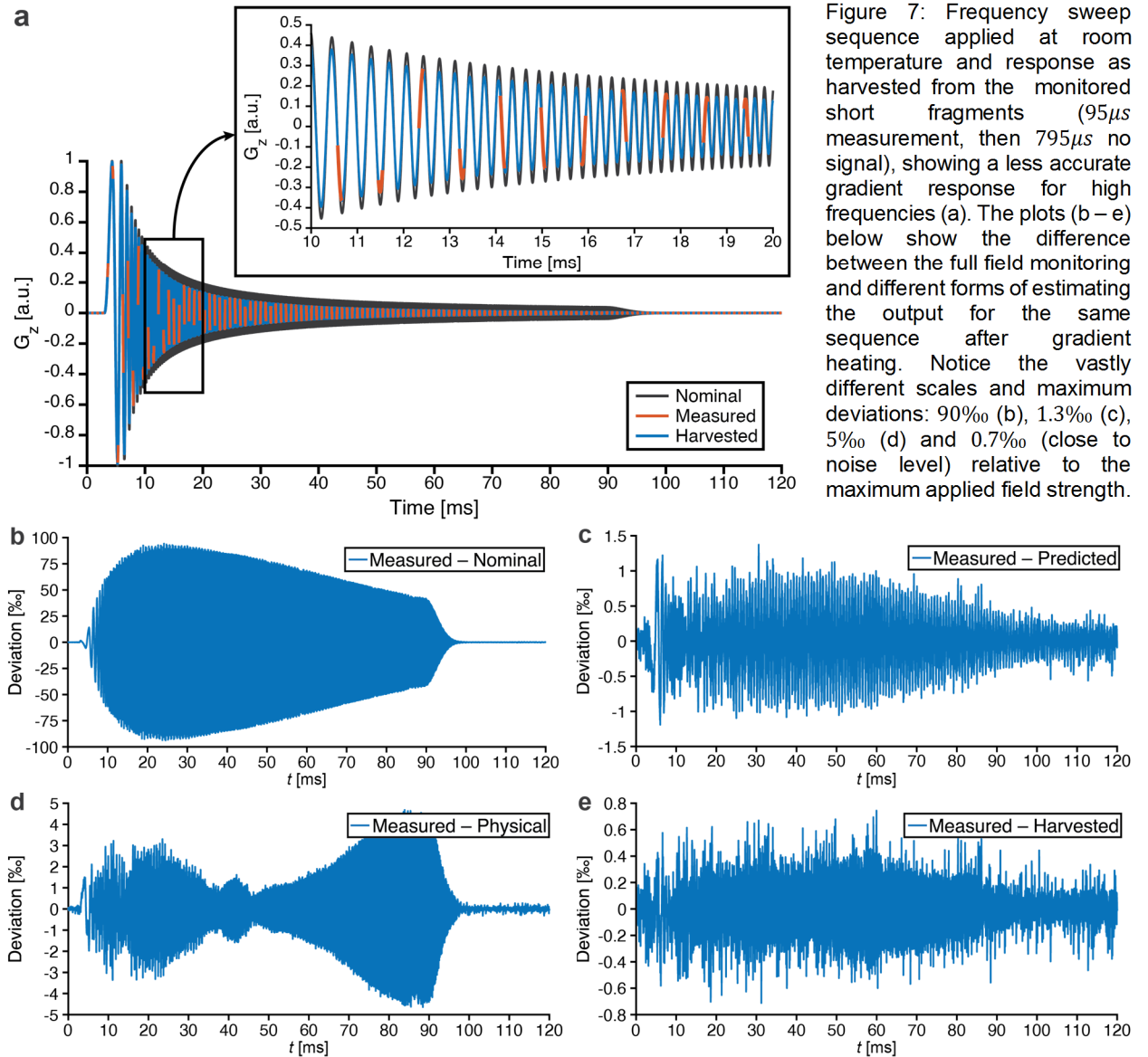


Figure 6: Intermediate stages of calculating an α GIRF: initial full response $G(\omega)$ (a), smoothed GIRF $\tilde{G}(\omega)$ (b), fitted oscillations $\tilde{G}(\omega) + G_{mv}(\omega)$ (c), final response $\alpha G(\omega) = G(\omega) - G_{mv}(\omega)$ (d).



Results

A comparison for different approaches for characterizing the gradient response from a single sequence measurement is shown in Figure 7. The frequency sweep allows characterization for a broad range of relevant frequencies (DC to 30kHz), though SNR decreases with increasing frequency due to lower attainable amplitude (2). No correction of gradient dynamics (b), other than system standard eddy current compensation (ECC), yields large errors (5% – 10% for low and over 100% relative error at high frequencies) demonstrating the need for further correction. The initial approach of using a purely physical model (c), without numerical

Figure 7: Frequency sweep sequence applied at room temperature and response as harvested from the monitored short fragments (95 μ s measurement, then 795 μ s no signal), showing a less accurate gradient response for high frequencies (a). The plots (b–e) below show the difference between the full field monitoring and different forms of estimating the output for the same sequence after gradient heating. Notice the vastly different scales and maximum deviations: 90‰ (b), 1.3‰ (c), 5‰ (d) and 0.7‰ (close to noise level) relative to the maximum applied field strength.

α GIRF, consisting only of eddy current and oscillation terms, could not accurately capture gradient dynamics for higher frequencies, suggesting the employed model is overly simplified and disregards potentially important aspects of the full response, such as amplifier BW limitations. A snapshot calibration method (d), provides better results, but cannot account for thermal drifts. This motivated the intermediate approach using a calibration (α GIRF) and physical model (Δ GIRF), achieving accurate characterization close to noise level of the monitored output over a broad temperature range (e).

Figure 8a displays a continuous unipolar blip waveform obtained by fitting the physical model to

the measured signal fragments, the nominal input is shown for comparison. Employing GIRF harvesting on such short isolated responses alone is hardly possible, given the low signal monitoring rate not being capable of providing enough information for a computational approach, e.g. in the analyzed response the $31\mu\text{s}$ pulse fell inside the $T_{gap} = 795\mu\text{s}$ gap between signal acquisitions. Doubling the monitoring rate, i.e. decreasing the time $T_{gap} = 345\mu\text{s}$, allowed in gaining enough information to provide for a slight adjustment of the physical parameters, however, these were not sufficient for exact characterization. The spectrally narrow oscillations were better characterized than broad eddy current effects (Figure 8b), since an

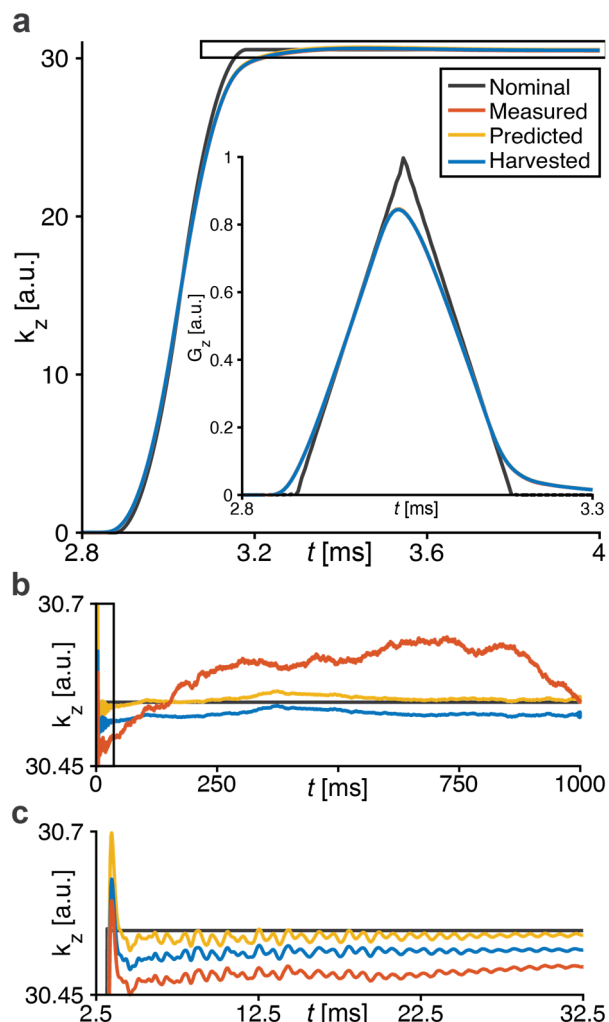


Figure 8: Response to triangular impulse predicted by a GIRF harvested in a prior sequence at high temperature (a). Close-up view of gradient drift (b) and oscillatory behaviour after the impulse (c).

insufficient amount of information during the actual impulse was measured in the single short acquisition window during the impulse, whereas the oscillations where measured during several following excitations over a longer time span. Comparing the output estimation given by the harvested response and the measured signal, we realize shortcomings of the investigated method. The estimated k -space step-response obtained from the response harvest displays a larger overshoot in comparison to the monitored signal, albeit smaller than the overshoot obtained in the predicted response using GIRF convolution in the calibration-based approach. The investigated method is unable to accurately characterize the thermal drifts occurring on a longer timescale due to the much faster field drifts measured in the response immediately after the applied impulse, preventing accurate optimization of the model parameters (Figure 8c). If sufficient data is available, as would be acquired in sequences with higher gradient activity, the optimization method yields rapidly converging solutions down to noise level, as displayed in other investigated sequences.

Nevertheless, considering the general trend to increased sequence encoding efficiency as a means to decrease scan time, the limitations addressed above do not pose a considerable hindrance. Rapid encoding sequences, such as EPI are well suited for GIRF harvesting since they provide significant output levels over extended periods of time, providing a basis for fast convergence and numerical stability of the optimization algorithm. The gradient response harvesting results for EPI sequences at two distinct temperatures are presented in Figure 9. Hereby it is notable that the characterization is not limited by noise level of individual probe acquisition fragments, a sub-noise level (relative to a single acquisition) characterization is achieved without filtering by mere virtue of using numerous such fragments for determining the numerical best-fit. On average 148 such fragments approximately $95\mu\text{s}$ in length were acquired for performing the optimization. The sparse acquisition captures enough information to accurately

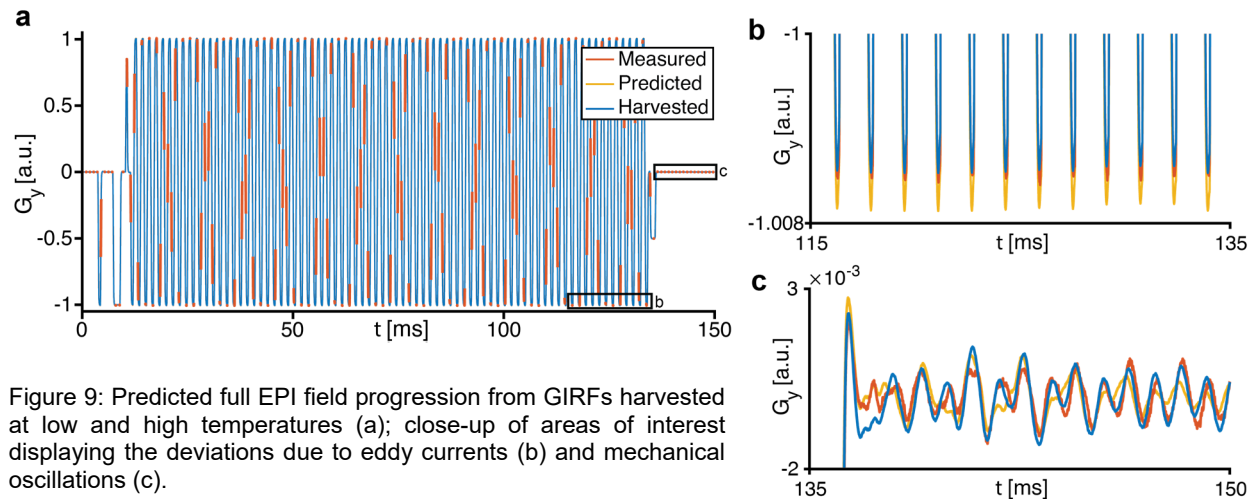


Figure 9: Predicted full EPI field progression from GIRFs harvested at low and high temperatures (a); close-up of areas of interest displaying the deviations due to eddy currents (b) and mechanical oscillations (c).

reconstruct the continuous gradient outputs in the transversal plane allowing k -space trajectory mapping, which would not be possible from the discontinuous monitored signal alone. Slight shifts in behavior between the low and high temperature outputs can be observed. The overall maximum error is around 0.08% of the peak field strength, which suffices even for demanding endeavors. Synchronicity issue between the sequence and the pulsed monitoring, such as in the case of measuring individual impulses displayed in Figure 8, might pose a

problem for the minimization due to the comb-like structure of the EPI pulses. It is possible to envisage a situation where the frequency of repeated gradient excitation coincides with a multiple of the pulsing frequency of the monitoring setup, however this was not encountered in the presented experiments. The responses obtained were utilized to calculate the k -space trajectory in the $X - Y$ plane which can be seen in Figure 10, comparing the concurrent field monitoring, calibration-based prediction and the investigated approach.

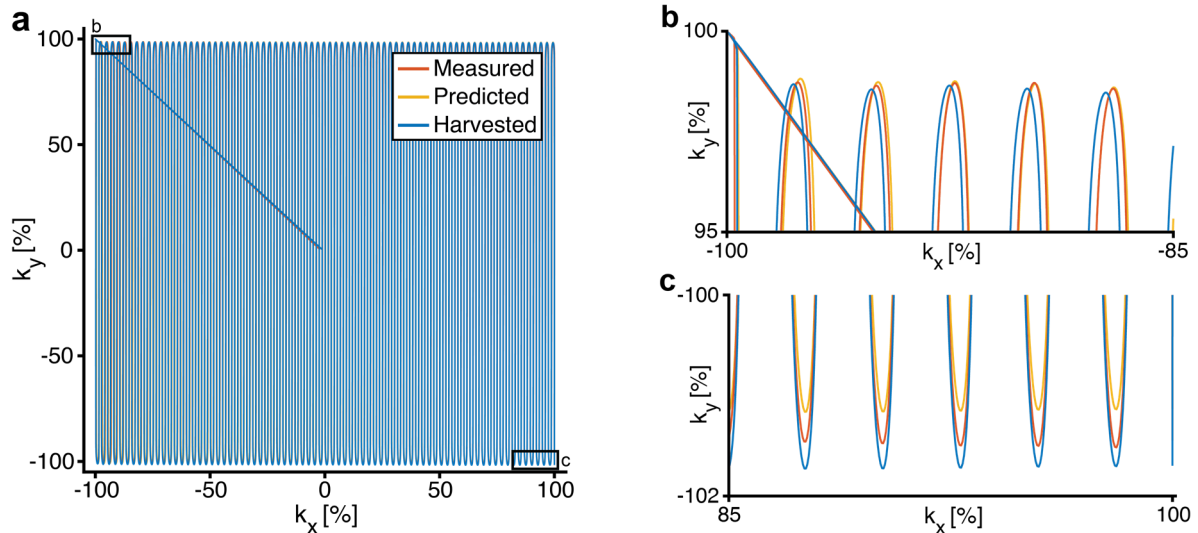


Figure 10: k -space trajectory based on GIRF harvested at a high temperature compared to concurrently monitored trajectory with a simple drift correction applied (a); close-up views (b,c).

Discussion

The concept of gradient impulse response harvesting, as introduced in (38), was constrained with

underlying system assumptions and evaluated. The proposed method of obtaining continuous field waveforms provides results closely matching those of continuous field monitoring within a maximum

error range of 0.07 % – 0.2% in terms of peak applied field strength for suitable sequences with high gradient activity or low switching frequency (as seen from Figure 7e), which is on the order typical thermal drift effects observed. Single-shot echo-planar and rapid 3D sequences could likely benefit, whereas other sequences are not feasible without adjustments to the method, however such a situation is not encountered frequently in typical use-cases. The result is achieved for a typical temperature range and with relaxed probe HW requirements. For first order gradient terms, a basic setup with a single set of $4 - 8$ ^1H or ^{19}F probes operating in a pulsed regime and allowing full relaxation between excitations would suffice to enable GIRF harvesting. The presented method can be seen as an intermediate between calibration-based output prediction and full sequence field monitoring. It provides a simple way to extend GIRF-based trajectory prediction to allow the use during scans where gradient heating is not negligible, and alleviates difficulties in continuous field monitoring setups by leveraging prior knowledge. This allowed a reduction of the monitoring rate from 86.4% to 11.95% without great loss of characterization quality. Hereby, the preliminary results suggest that the utilized model accounts in large parts for gradient behavior caused by heating and that sufficient description of such effects might be achieved with a very small number of 2 – 4 eddy current terms.

The method was sufficiently accurate to characterize important vibration peaks in the response at different temperatures. Real-time preemphasis tuning using the harvested physical parameters, sequence design, improving results of non-Cartesian or fast imaging procedures and real-time system diagnostics are some prospective applications where harvesting could prove beneficial. Combining with field feedback to address non-linear field deviations, e.g. through patient movement, appears attractive and further research is called for. By also incorporating advanced image reconstruction, such as algebraic higher order schemes (9,42), it would be possible to reduce gradient HW requirements while retaining high image quality, thereby reducing costs through the use of sophisticated computation instead of relying on gradient

response fidelity. The developed method is based on the assumption of an existing decomposition of the full response into an LTI and a slow time-variant response contribution with gradual shifts in parameters of the underlying physical model. The LTI response can hereby be determined by various methods in a calibration step, however, to enable fully concurrent characterization without any prior measurement, this would optimally be performed with the same setup at the beginning of a given scan session.

Given the difficulties encountered in determining the full response based on the proposed physical model, a purely numerical approach could be used to achieve the initial characterization (38). For the time-varying response, the parameters are adapted according to numerical fitting of the model to infrequent field measurements. Several restrictions might apply with the above assumptions. Primarily, there is no way to guarantee that the recorded trajectory fragments will include all spectral components necessary for trajectory reconstruction, regardless of the acquisition length. Important effects could be hereby lost. In particular, a situation where the monitoring frequency and duration is matched with gradient switching of a particular sequence, in such a way that each acquired fragment provides no new spectral information during an update period T_p . This issue could be mitigated by using pseudo-random gap durations instead of fixed values in some cases. In other cases, this possibly poses an inherent restriction, thus limiting applicability. Such a situation has been encountered for sequences consisting solely of single unipolar blips. However, for long and repetitive sequences such as the EPI sequence used for validation, the results suggest that this is not an issue, but further validation with different sequences is necessary. Lower and upper limits of the response update frequency T_p based on desired performance would need to be assessed in the future. Hereby, the speed and robustness criteria of the numerical optimization are likely to yield a lower limit of this value. This additionally provide an area for possible improvement, where algorithms commonly applied to different problems may be suitable. Given the presented LR and RLC models for

eddy current and vibration characterization, it could be worthwhile considering optimization algorithms employed in analog RLC filter design (43). Ultimately, the preliminary results of this novel approach appear promising, but further validation is necessary. Particularly, there is a lack of image reconstruction results, which are crucial for comprehensive assessment and would hence be a plausible next step.

References

- (1) P. C. Lauterbur, "Image formation by induced local interactions. Examples employing nuclear magnetic resonance," *Nat. (London, United Kingdom)*, vol. 242, pp. 190–191, 1973.
- (2) S. J. Vennesjo, B. E. Dietrich, M. Pavan, D. O. Brunner, B. J. Wilm, C. Barmet, and K. P. Pruessmann, "Field camera measurements of gradient and shim impulse responses using frequency sweeps," *Magn. Reson. Med.*, vol. 72, no. 2, pp. 570–583, 2014.
- (3) E. K. Brodsky, A. A. Samsonov, and W. F. Block, "Characterizing and correcting gradient errors in non-Cartesian imaging: Are gradient errors Linear Time-Invariant (LTI)?," *Magn. Reson. Med.*, vol. 62, no. 6, pp. 1466–1476, 2009.
- (4) P. Jehenson, M. Westphal, and N. Schuff, "Analytical method for the compensation of eddy-current effects induced by pulsed magnetic field gradients in NMR systems," *J. Magn. Reson.*, vol. 90, no. 2, pp. 264–278, Nov. 1990.
- (5) J. J. Van Vaals and A. H. Bergman, "Optimization of eddy-current compensation," *J. Magn. Reson.*, vol. 90, no. 1, pp. 52–70, 1990.
- (6) A. H. Bergman and J. J. van Vaals, "Optimization of Eddy-Current Compensation," *J. Magn. Reson.*, vol. 90, pp. 52–70, 1990.
- (7) C. Boesch, R. Gruetter, and E. Martin, "Temporal and spatial analysis of fields generated by eddy currents in superconducting magnets: optimization of corrections and quantitative characterization of magnet/gradient systems.," *Magn. Reson. Med.*, vol. 20, no. 2, pp. 268–84, 1991.
- (8) Y. Wu, B. a Chronik, C. Bowen, C. K. Mechefske, and B. K. Rutt, "Gradient-induced acoustic and magnetic field fluctuations in a 4T whole- body MR imager," *Magn Reson Med*, vol. 44, no. 4, p. 532–6., 2000.
- (9) B. J. Wilm, C. Barmet, M. Pavan, and K. P. Pruessmann, "Higher order reconstruction for MRI in the presence of spatiotemporal field perturbations," *Magn. Reson. Med.*, vol. 65, no. 6, pp. 1690–1701, 2011.
- (10) C. Barmet, B. Wilm, and M. Pavan, "Concurrent higher-order field monitoring for routine head MRI: an integrated heteronuclear setup," *Proc. ISMRM*, vol. 18, no. 2008, p. 216, 2010.
- (11) Y. Duerst, B. J. Wilm, B. E. Dietrich, S. J. Vannesjo, C. Barmet, T. Schmid, D. O. Brunner, and K. P. Pruessmann, "Real-time feedback for spatiotemporal field stabilization in MR systems," *Magn. Reson. Med.*, vol. 73, no. 2, pp. 884–893, 2015.
- (12) S. J. Vannesjo, B. J. Wilm, Y. Duerst, S. Gross, D. O. Brunner, B. E. Dietrich, T. Schmid, C. Barmet, and K. P. Pruessmann, "Retrospective correction of physiological field fluctuations in high-field brain MRI using concurrent field monitoring," *Magn. Reson. Med.*, vol. 73, no. 5, pp. 1833–1843, 2015.
- (13) S. J. Vannesjo, M. Haeberlin, L. Kasper, M. Pavan, B. J. Wilm, C. Barmet, and K. P. Pruessmann, "Gradient system characterization by impulse response measurements with a dynamic field camera," *Magn. Reson. Med.*, vol. 69, no. 2, pp. 583–593, 2013.
- (14) S. B. Reeder, E. Atalar, B. D. Bolster, and E. R. McVeigh, "Quantification and reduction of ghosting artifacts in interleaved echo- planar imaging," *Magn. Reson. Med.*, vol. 38, no. 3, pp. 429–439, 1997.
- (15) L. Kasper, S. Bollmann, S. J. Vannesjo, S. Gross, M. Haeberlin, B. E. Dietrich, and K. P. Pruessmann, "Monitoring, analysis, and correction of magnetic field fluctuations in echo planar imaging time series," *Magn. Reson. Med.*, vol. 40, pp. 396–409, 2014.
- (16) C. B. Ahn, J. H. Kim, and Z. H. Cho, "High-speed spiral-scan echo planar NMR imaging-I.," *IEEE Trans. Med. Imaging*, vol. 5, no. 1, pp. 2–7, 1986.
- (17) J. Busch, S. J. Vannesjo, C. Barmet, K. P. Pruessmann, and S. Kozerke, "Analysis of temperature dependence of background phase errors in phase-contrast cardiovascular magnetic resonance.," *J. Cardiovasc. Magn. Reson.*, vol. 16, p. 97, 2014.
- (18) A. Henning, C. Barmet, A. Fuchs, J. Vannesjö, P. Boesiger, and K. P. Pruessmann, "Characterization and correction of modulation sidebands in 1H MRS without water suppression by spatiotemporal field monitoring," *Proc. ISMRM*, no. 41, p. 2009, 2009.

Acknowledgements

The help of Benjamin Dietrich for the use of the experimental setup and providing data for methods evaluation and comparison is gratefully acknowledged. Gratitude is also due for the supervisor of the work, Bertram Wilm, without whose guidance and tremendous patience this project would not have been possible.

- (19) P. Jezzard and S. Clare, "Sources of Distortions in Functional MRI Data," *Hum. Brain Mapp.*, vol. 8, no. May, pp. 80–85, 1999.
- (20) B. J. Wilm, Z. Nagy, C. Barmet, S. J. Vannesjo, L. Kasper, M. Haeberlin, S. Gross, B. E. Dietrich, D. O. Brunner, T. Schmid, and K. P. Pruessmann, "Diffusion MRI with concurrent magnetic field monitoring," *Magn. Reson. Med.*, vol. 74, no. 4, pp. 925–933, 2015.
- (21) G. F. Mason, T. Harshbarger, H. P. Hetherington, Y. Zhang, G. M. Pohost, and D. B. Twieg, "A method to measure arbitrary k-space trajectories for rapid MR imaging," *Magn. Reson. Med.*, vol. 38, no. 3, pp. 492–496, 1997.
- (22) T. W. Nixon, S. McIntyre, D. L. Rothman, and R. A. de Graaf, "Compensation of gradient-induced magnetic field perturbations," *J. Magn. Reson.*, vol. 192, no. 2, pp. 209–217, Jun. 2008.
- (23) H. Liu and G. B. Matson, "Accurate measurement of magnetic resonance imaging gradient characteristics," *Materials (Basel)*, vol. 7, no. 1, pp. 1–15, 2014.
- (24) A. E. Campbell-Washburn, H. Xue, R. J. Lederman, A. Z. Faranesh, and M. S. Hansen, "Real-time distortion correction of spiral and echo planar images using the gradient system impulse response function," *Magn. Reson. Med.*, vol. 75, no. 6, pp. 2278–2285, Jun. 2016.
- (25) S. J. Vannesjo, "A Method for Characterizing the Magnetic Field Response of a Gradient System," in *Proceedings of the ISMRM*, 2010, no. 2010.
- (26) Y. Zhang, H. P. Hetherington, E. M. Stokely, G. F. Mason, and D. B. Twieg, "A novel k-space trajectory measurement technique," *Magn. Reson. Med.*, vol. 39, no. 6, pp. 999–1004, 1998.
- (27) M. T. Alley, G. H. Glover, and N. J. Pelc, "Gradient characterization using a fourier-transform technique," *Magn. Reson. Med.*, vol. 39, no. 4, pp. 581–587, 1998.
- (28) K. P. Pruessmann, C. Barmet, and N. De Zanche, "Magnetic Field Monitoring during MRI Acquisition Improves Image Reconstruction," in *Proceedings of the ISMRM*, 2005, vol. 132, p. 681.
- (29) C. Barmet, N. De Zanche, and K. P. Pruessmann, "Spatiotemporal magnetic field monitoring for MR," *Magn. Reson. Med.*, vol. 60, no. 1, pp. 187–197, 2008.
- (30) N. De Zanche, C. Barmet, J. A. Nordmeyer-Massner, and K. P. Pruessmann, "NMR Probes for measuring magnetic fields and field dynamics in MR systems," *Magn. Reson. Med.*, vol. 60, no. 1, pp. 176–186, 2008.
- (31) C. Barmet, N. De Zanche, B. J. Wilm, and K. P. Pruessmann, "A transmit/receive system for magnetic field monitoring of in vivo MRI," *Magn. Reson. Med.*, vol. 62, no. 1, pp. 269–276, 2009.
- (32) P. Sipilä, S. Greding, G. Wachutka, and F. Wiesinger, "2H transmit-receive NMR probes for magnetic field monitoring in MRI," *Magn. Reson. Med.*, vol. 65, no. 5, pp. 1498–1506, 2011.
- (33) P. Sipilä, G. Wachutka, and F. Wiesinger, "Coherent excitation scheme to operate pulsed NMR probes for real-time magnetic field monitoring," in *Proceedings of the ISMRM*, 2010, vol. 145, p. 3076.
- (34) D. O. Brunner, B. E. Dietrich, M. Çavuşoğlu, B. J. Wilm, T. Schmid, S. Gross, C. Barmet, and K. P. Pruessmann, "Concurrent recording of RF pulses and gradient fields - comprehensive field monitoring for MRI," *NMR Biomed.*, vol. 29, no. 9, pp. 1162–1172, Sep. 2016.
- (35) B. E. Dietrich, D. O. Brunner, B. J. Wilm, C. Barmet, and K. P. Pruessmann, "Continuous Magnetic Field Monitoring Using Rapid Re-Excitation of NMR Probe Sets," *IEEE Trans. Med. Imaging*, vol. 35, no. 6, pp. 1452–1462, Jun. 2016.
- (36) N. De Zanche, C. Barmet, J. A. Massner, and K. P. Pruessmann, "Advances in NMR Probe Technology for Magnetic Field Monitoring," in *Proceedings of the ISMRM*, 2006, vol. 132, no. 5244, p. 781.
- (37) C. Barmet, N. De Zanche, B. Wilm, and K. Pruessmann, "Towards routine field monitoring for MRI: a transmit/receive system based on shielded NMR probes," *Proc. 16th Sci. Meet. Int. Soc. Magn. Reson. Med.*, vol. Toronto, no. 5244, p. 1152, 2008.
- (38) B. J. Wilm, "Gradient response harvesting for continuous system characterization during MR sequences," in *Proceedings of the ISMRM*, 2016, no. 544.
- (39) M. a Bernstein, K. E. King, X. J. Zhou, and W. Fong, *Handbook of MRI Pulse Sequences*, vol. 32, no. 5. 2005.
- (40) S. A. Counter, A. Olofsson, H. F. Grahn, and E. Borg, "MRI acoustic noise: Sound pressure and frequency analysis," *J. Magn. Reson. Imaging*, vol. 7, no. 3, pp. 606–611, 1997.
- (41) B. E. Dietrich, D. O. Brunner, B. J. Wilm, C. Barmet, S. Gross, L. Kasper, M. Haeberlin, T. Schmid, S. J. Vannesjo, and K. P. Pruessmann, "A field camera for MR sequence monitoring and system analysis," *Magn. Reson. Med.*, vol. 0, p. n/a-n/a, 2015.
- (42) B. J. Wilm, C. Barmet, and K. P. Pruessmann, "Fast higher-order MR image reconstruction using singular-vector separation," *IEEE Trans. Med. Imaging*, vol. 31, no. 7, pp. 1396–1403, 2012.
- (43) A. G. Radwan and M. E. Fouad, "Optimization of fractional-order RLC filters," *Circuits, Syst. Signal Process.*, vol. 32, no. 5, pp. 2097–2118, 2013.

The source code is available under: <https://polybox.ethz.ch/index.php/s/FEM1MUtyzbQqz5x> (Password: alphaGIRF)